Physica A 387 (2008) 4787–4799

Contents lists available at ScienceDirect

Physica A

journal homepage: www.elsevier.com/locate/physa

A second-order accurate non-linear difference scheme for the *N*-component Cahn–Hilliard system

Hyun Geun Lee, Junseok Kim *

Department of Mathematics, Korea University, Seoul 136-701, Republic of Korea

ARTICLE INFO

Article history:
Received 10 January 2008
Received in revised form 17 March 2008
Available online 28 March 2008

Keywords:
N-component Cahn–Hilliard
Nonlinear multigrid
Phase separation
Finite difference

ABSTRACT

We consider a second-order conservative nonlinear numerical scheme for the *N*-component Cahn–Hilliard system modeling the phase separation of a *N*-component mixture. The scheme is based on a Crank–Nicolson finite-difference method and is solved by an efficient and accurate nonlinear multigrid method. We numerically demonstrate the second-order accuracy of the numerical scheme. We observe that our numerical solutions are consistent with the exact solutions of linear stability analysis results. We also describe numerical experiments such as the evolution of triple junctions and the spinodal decomposition in a quaternary mixture. We investigate the effects of a concentration dependent mobility on phase separation.

1. Introduction

In this paper, we consider an efficient and accurate numerical method of a model for phase separation in a *N*-component mixture. When a homogeneous system composed of *N*-components, at high temperature, is rapidly cooled to a uniform temperature below a critical temperature, where it is unstable with respect to concentration fluctuations, spinodal decomposition [7] takes place: The system separates into spatial regions rich in one component and poor in the other components. It evolves into an equilibrium state with lower overall free energy [9].

Spinodal decomposition is of interest on two counts. First, it is one of the few solid-state transformations for which there is any plausible quantitative theory. Second, from a practical viewpoint, spinodal decomposition is of interest because it affords a means of producing a very finely dispersed structure that can enhance the properties of a material [22].

Most of the technologically important alloys are multi-component systems exhibiting multiple phases in their microstructures. Moreover, one or more of these phases are formed as a result of phase transformations induced during processing. Since the performance of these multi-component alloys depends crucially on the morphology of the phase, a fundamental understanding of the kinetics of phase transformations is important for controlling the microstructures of these multi-phase alloys [1].

Cahn [6] extended the van der Waals model [31] to time-dependent problems by approximating the interfacial diffusion as being proportional to chemical potential gradients. Generalization of the Cahn–Hilliard (CH) equations to multi-component systems appeared with de Fontaine [17] and Morral and Cahn [26]. Elliott and Luckhaus [15] gave a global existence result under constant mobility and specific assumptions on the form of the free energy. Elliott and Garcke [13] developed an existence theory for multi-component diffusion when the mobility matrix depends on the order parameters. Differences between binary and multi-component alloys were identified and the equilibrium and dynamic behavior of multi-component systems were studied by Eyre [16].

* Corresponding author. Tel.: +82 2 3290 3077.
E-mail addresses: leeh@dongguk.edu (H.G. Lee), cfdkim@korea.ac.kr (J. Kim).

0378-4371/$ – see front matter © 2008 Elsevier B.V. All rights reserved.
doi:10.1016/j.physa.2008.03.023

Although there are many numerical studies (see Refs. [2,10–12,14,18–20,29] and references therein) with binary CH equation and ternary CH equation [4,9,16,25,28], much less has been conducted on the quaternary CH system. In Ref. [24], vector-valued Allen-Cahn equations were considered. In Ref. [27], multi-component fluid mixtures were studied using molecular dynamics. In Ref. [25], a finite difference method is used for the constant mobility. In Ref. [3], a finite element approximation is used for the ternary CH system with a degenerate mobility matrix.

The purpose of this work is to consider a conservative second-order accurate nonlinear numerical method for the N-component CH system with concentration dependent mobility for a N-component mixture.

The contents of this paper are as follows. In Section 2 we briefly review governing equations for phase separation in a N-component system which takes a concentration dependence of the mobility. In Section 3 we consider a fully discrete semi-implicit finite difference scheme and describe an efficient and accurate nonlinear multigrid V-cycle algorithm for the N-component CH system. We present numerical experiments such as a second-order convergence test, comparison with a linear stability analysis of the equations, the evolution of triple junctions, and phase separation in a quaternary mixture in Section 4. Finally, in Section 5 we conclude.

2. Governing equations

We consider a system of a N-component mixture. Let $c_i = c_i(\mathbf{x}, t)$ for $i = 1, \ldots, N$ be the mole fraction of the ith component in the mixture as a function of space and time. Clearly the total mole fractions must sum to 1, i.e.,

$$c_1 + c_2 + \cdots + c_N = 1, \tag{1}$$

so that, admissible states belong to the Gibbs N-simplex

$$GS := \left\{ (c_1, c_2, \ldots, c_N) \in \mathbb{R}^N \,\middle|\, \sum_{i=1}^{N} c_i = 1,\ 0 \le c_i \le 1 \text{ for } i = 1, \ldots, N \right\}.$$

Let $\mathbf{c} = (c_1, c_2, \ldots, c_N)$ be a vector valued phase field. Without loss of generality, we choose a Helmholtz free energy functional $\mathcal{F}$ of a generalized Ginzburg-Landau form

$$\mathcal{F}(t) = \mathcal{F}(\mathbf{c}(\mathbf{x}, t)) = \int_\Omega \left(F(\mathbf{c}) + \frac{\epsilon^2}{2} \sum_{i=1}^{N} |\nabla c_i|^2 \right) \mathrm{d}\mathbf{x}, \tag{2}$$

where Ω is an open domain in $\mathbb{R}^d$ ($d \in \mathbb{N}$). The homogenous free energy is defined as $F(\mathbf{c}) = \frac{1}{4}\sum_{i=1}^{N} c_i^2(1 - c_i)^2$ and ϵ is the gradient energy coefficient. The natural boundary condition for the N-component CH system is the zero Neumann boundary condition:

$$\nabla c_i \cdot \mathbf{n} = 0 \text{ on } \partial\Omega, \tag{3}$$

where $\mathbf{n}$ is the unit normal vector to $\partial\Omega$.

The time evolution of $\mathbf{c}$ is governed by the gradient of the energy with respect to the H_o^{-1} inner product under the additional constraint (1), which has to hold everywhere at any time. In order to ensure this last constraint, we use a variable Lagrange multiplier $\beta(\mathbf{c})$ [21] and set $\frac{\partial F}{\partial \mathbf{c}} = \left(\frac{\partial F}{\partial c_1}, \frac{\partial F}{\partial c_2}, \ldots, \frac{\partial F}{\partial c_N} \right) = \mathbf{f}(\mathbf{c}) = (f(c_1), f(c_2), \ldots, f(c_N))$, where $f(c) = c(c-0.5)(c-1)$. Let $\mathbf{1} = (1, \ldots, 1) \in \mathbb{R}^N$ and $\mathbf{e}_i$ be the vector of length N, which has a 1 only in the ith coordinate and zeros elsewhere. Using a general smooth vector valued function $\boldsymbol{\zeta}$, we set

$$\mathbf{d} = (d_1, d_2, \ldots, d_N) = \boldsymbol{\zeta} - \frac{1}{N}\sum_{i=1}^{N} \zeta_i \mathbf{1}, \quad \text{then } \sum_{i=1}^{N} d_i = 0.$$

Let

$$\beta(\mathbf{c}) = -\frac{1}{N}\sum_{i=1}^{N} f(c_i). \tag{4}$$

Then, we have the following

$$\begin{aligned}
\frac{\mathrm{d}}{\mathrm{d}\eta}\mathcal{F}(\mathbf{c} + \eta\mathbf{d})|_{\eta=0} &= \frac{\mathrm{d}}{\mathrm{d}\eta} \int_\Omega \sum_{i=1}^{N} \left(\frac{1}{4}(c_i + \eta d_i)^2(1 - (c_i + \eta d_i))^2 + \frac{\epsilon^2}{2}|\nabla(c_i + \eta d_i)|^2 \right) \mathrm{d}\mathbf{x} \Big|_{\eta=0} \\
&= \int_\Omega \sum_{i=1}^{N} \left(d_i f(c_i) + \epsilon^2 \nabla d_i \cdot \nabla c_i \right) \mathrm{d}\mathbf{x} \\
&= \int_\Omega \left[\mathbf{f}(\mathbf{c}) \cdot \boldsymbol{\zeta} - \mathbf{f}(\mathbf{c}) \cdot \frac{1}{N}\sum_{i=1}^{N} \zeta_i \mathbf{1} + \epsilon^2 \sum_{i=1}^{N} \nabla \left(\zeta_i - \frac{1}{N}\sum_{j=1}^{N} \zeta_j \right) \cdot \nabla c_i \right] \mathrm{d}\mathbf{x} \\
&= \int_\Omega \left[\mathbf{f}(\mathbf{c}) \cdot \boldsymbol{\zeta} + \beta(\mathbf{c})\mathbf{1} \cdot \boldsymbol{\zeta} + \epsilon^2 \sum_{i=1}^{N} \left(\nabla\zeta_i \cdot \nabla c_i - \frac{1}{N}\nabla \sum_{j=1}^{N} \zeta_j \cdot \nabla c_i \right) \right] \mathrm{d}\mathbf{x}
\end{aligned}$$

$$
\begin{aligned}
&= \int_\Omega (\mathbf{f}(\mathbf{c}) + \beta(\mathbf{c})\mathbf{1}) \cdot \boldsymbol{\zeta}\, \mathrm{d}\mathbf{x} \\
&\quad + \epsilon^2 \sum_{i=1}^{N} \left[\int_{\partial\Omega} \left(\zeta_i \nabla c_i - \frac{1}{N} \sum_{j=1}^{N} \zeta_j \nabla c_i \right) \cdot \mathbf{n}\, \mathrm{d}s - \int_\Omega \left(\zeta_i \Delta c_i - \frac{1}{N} \sum_{j=1}^{N} \zeta_j \Delta c_i \right) \mathrm{d}\mathbf{x} \right] \\
&= \int_\Omega (\mathbf{f}(\mathbf{c}) + \beta(\mathbf{c})\mathbf{1}) \cdot \boldsymbol{\zeta}\, \mathrm{d}\mathbf{x} - \epsilon^2 \int_\Omega \sum_{i=1}^{N} \left(\zeta_i \Delta c_i - \frac{1}{N} \sum_{j=1}^{N} \zeta_j \Delta c_i \right) \mathrm{d}\mathbf{x} \\
&= \int_\Omega \left(\mathbf{f}(\mathbf{c}) - \epsilon^2 \Delta \mathbf{c} + \beta(\mathbf{c})\mathbf{1} \right) \cdot \boldsymbol{\zeta}\, \mathrm{d}\mathbf{x} = \int_\Omega (\mu_1, \mu_2, \ldots, \mu_N) \cdot \boldsymbol{\zeta}\, \mathrm{d}\mathbf{x},
\end{aligned}
$$

where we have used the boundary condition (3). Now we get the chemical potential $\boldsymbol{\mu} = (\mu_1, \mu_2, \ldots, \mu_N) = \mathbf{f}(\mathbf{c}) - \epsilon^2 \Delta \mathbf{c} + \beta(\mathbf{c})\mathbf{1}$ as the variational derivative of $\mathcal{F}$ with respect to $\mathbf{c}$. The governing equations for the phase fields describe the rate of each phase change in the system. Ensuring that the total free energy $\mathcal{F}$ decreases monotonically and the total mass is conserved in time, these evolution equations can be derived from the gradient flow of $\mathcal{F}$.

$$
\frac{\partial c_i}{\partial t} = \nabla \cdot (M(\mathbf{c}) \nabla \mu_i), \tag{5}
$$

$$
\mu_i = f(c_i) - \epsilon^2 \Delta c_i + \beta(\mathbf{c}), \quad \text{for } i = 1, 2, \ldots, N, \tag{6}
$$

where

$$
M(\mathbf{c}) = \sum_{i<j}^{N} c_i c_j
$$

is the concentration dependent mobility. The mass conserving boundary condition for the system is

$$
\nabla \mu_i \cdot \mathbf{n} = 0 \quad \text{on } \partial\Omega. \tag{7}
$$

We differentiate the energy $\mathcal{F}$ and the total mass of each phase, $\int_\Omega c_i \mathrm{d}\mathbf{x}$, to get

$$
\begin{aligned}
\frac{\mathrm{d}}{\mathrm{d}t} \mathcal{F}(t) &= \int_\Omega \sum_{i=1}^{N} \left(\frac{\partial F(\mathbf{c})}{\partial c_i} \frac{\partial c_i}{\partial t} + \epsilon^2 \nabla c_i \cdot \nabla \frac{\partial c_i}{\partial t} \right) \mathrm{d}\mathbf{x} \\
&= \int_\Omega \sum_{i=1}^{N} \frac{\partial F(\mathbf{c})}{\partial c_i} \frac{\partial c_i}{\partial t} \mathrm{d}\mathbf{x} + \int_{\partial\Omega} \sum_{i=1}^{N} \epsilon^2 \nabla c_i \cdot \mathbf{n} \frac{\partial c_i}{\partial t} \mathrm{d}s - \int_\Omega \sum_{i=1}^{N} \epsilon^2 \Delta c_i \frac{\partial c_i}{\partial t} \mathrm{d}\mathbf{x} \\
&= \int_\Omega \sum_{i=1}^{N} \left(\frac{\partial F(\mathbf{c})}{\partial c_i} - \epsilon^2 \Delta c_i \right) \frac{\partial c_i}{\partial t} \mathrm{d}\mathbf{x} = \int_\Omega \sum_{i=1}^{N} (\mu_i - \beta(\mathbf{c})) \frac{\partial c_i}{\partial t} \mathrm{d}\mathbf{x} \\
&= \int_\Omega \sum_{i=1}^{N} \mu_i \nabla \cdot (M(\mathbf{c}) \nabla \mu_i) \mathrm{d}\mathbf{x} - \beta(\mathbf{c}) \int_\Omega \sum_{i=1}^{N} \frac{\partial c_i}{\partial t} \mathrm{d}\mathbf{x} = - \int_\Omega M(\mathbf{c}) \sum_{i=1}^{N} |\nabla \mu_i|^2 \mathrm{d}\mathbf{x} \le 0
\end{aligned}
$$

and

$$
\frac{\mathrm{d}}{\mathrm{d}t} \int_\Omega c_i \mathrm{d}\mathbf{x} = \int_\Omega \frac{\partial c_i}{\partial t} \mathrm{d}\mathbf{x} = \int_\Omega \nabla \cdot (M(\mathbf{c}) \nabla \mu_i)\, \mathrm{d}\mathbf{x} = \int_{\partial\Omega} M(\mathbf{c}) \nabla \mu_i \cdot \mathbf{n} \mathrm{d}s = 0,
$$

where we used the mass conserving boundary condition (7). Therefore, the total energy is non-increasing in time ($\mathcal{F}(t)$ is a Lyapunov functional of the N-component CH system) and the total mass of each phase is conserved. That is

$$
\mathcal{F}(t) \le \mathcal{F}(0) \quad \text{and} \quad \int_\Omega c_i(\mathbf{x}, t) \mathrm{d}\mathbf{x} = \int_\Omega c_i(\mathbf{x}, 0) \mathrm{d}\mathbf{x} \quad \text{for } i = 1, \ldots, N.
$$

3. Numerical solution

Since $c_N = 1 - c_1 - c_2 - \cdots - c_{N-1}$ for N-component systems, we only need to solve the equations with $c_1, c_2, \ldots$, and c_{N-1}. Let $\mathbf{c} = (c_1, c_2, \ldots, c_{N-1})$ and $\boldsymbol{\mu} = (\mu_1, \mu_2, \ldots, \mu_{N-1})$. In the following numerical scheme and solution algorithm, we restrict space dimensions to two for simplicity. The three-dimensional extension is straightforward.

3.1. Discretization

Let $\Omega = [a, b] \times [c, d] \subset \mathbb{R}^2$ be partitioned by

$$
\begin{aligned}
&a = x_{\frac{1}{2}} < x_{1+\frac{1}{2}} < \cdots < x_{N_x-1+\frac{1}{2}} < x_{N_x+\frac{1}{2}} = b, \\
&c = y_{\frac{1}{2}} < y_{1+\frac{1}{2}} < \cdots < y_{N_y-1+\frac{1}{2}} < y_{N_y+\frac{1}{2}} = d.
\end{aligned}
$$

For simplicity, we assume the above partitions are uniform in both directions and the grid size is h. We denote by $\Omega_h = \{(x_i, y_j) : 1 \le i \le N_x, \quad 1 \le j \le N_y\}$ a set of cell centered points $(x_i, y_j) = ((x_{i-\frac{1}{2}} + x_{i+\frac{1}{2}})/2, (y_{j-\frac{1}{2}} + y_{j+\frac{1}{2}})/2)$.

Let $\mathbf{c}_{ij}$ and $\boldsymbol{\mu}_{ij}$ be approximations of $\mathbf{c}(x_i, y_j)$ and $\boldsymbol{\mu}(x_i, y_j)$. We first implement the zero Neumann boundary condition (3) by requiring that

$$D_x\mathbf{c}_{\frac{1}{2},j} = D_x\mathbf{c}_{N_x+\frac{1}{2},j} = D_y\mathbf{c}_{i,\frac{1}{2}} = D_y\mathbf{c}_{i,N_y+\frac{1}{2}} = \mathbf{0},$$
$$D_x\boldsymbol{\mu}_{\frac{1}{2},j} = D_x\boldsymbol{\mu}_{N_x+\frac{1}{2},j} = D_y\boldsymbol{\mu}_{i,\frac{1}{2}} = D_y\boldsymbol{\mu}_{i,N_y+\frac{1}{2}} = \mathbf{0},$$

where the discrete differentiation operators are

$$D_x\mathbf{c}_{i+\frac{1}{2},j} = (\mathbf{c}_{i+1,j} - \mathbf{c}_{ij})/h \quad \text{and} \quad D_y\mathbf{c}_{i,j+\frac{1}{2}} = (\mathbf{c}_{i,j+1} - \mathbf{c}_{ij})/h.$$

We then define the discrete Laplacian by

$$\Delta_d\mathbf{c}_{ij} = (D_x\mathbf{c}_{i+\frac{1}{2},j} - D_x\mathbf{c}_{i-\frac{1}{2},j} + D_y\mathbf{c}_{i,j+\frac{1}{2}} - D_y\mathbf{c}_{i,j-\frac{1}{2}})/h$$

and the discrete l^2 inner product by

$$(\mathbf{c}, \mathbf{d})_h = h^2 \sum_{i=1}^{N_x}\sum_{j=1}^{N_y}(c_{1ij}d_{1ij} + c_{2ij}d_{2ij} + \cdots + c_{N-1ij}d_{N-1ij}). \tag{8}$$

We also define a discrete norm associated with (8) as

$$\|\mathbf{c}\|^2 = (\mathbf{c}, \mathbf{c})_h.$$

We redefine $\mathbf{f}(\mathbf{c})$ and $\mathbf{1}$ to $\mathbf{f}(\mathbf{c}) = (f(c_1), f(c_2), \ldots, f(c_{N-1}))$ and $\mathbf{1} = (1, \ldots, 1) \in \mathbb{R}^{N-1}$. We discretize Eqs. (5) and (6) in time by the Crank–Nicolson algorithm:

$$\frac{\mathbf{c}_{ij}^{n+1} - \mathbf{c}_{ij}^{n}}{\Delta t} = \nabla_d \cdot (M^{n+\frac{1}{2}}\nabla_d\boldsymbol{\mu}_{ij}^{n+\frac{1}{2}}), \tag{9}$$

$$\boldsymbol{\mu}_{ij}^{n+\frac{1}{2}} = \frac{1}{2}(\boldsymbol{\varphi}(\mathbf{c}_{ij}^{n+1}) + \boldsymbol{\varphi}(\mathbf{c}_{ij}^{n})) - \frac{\epsilon^2}{2}\Delta_d(\mathbf{c}_{ij}^{n+1} + \mathbf{c}_{ij}^{n}), \tag{10}$$

where the nonlinear function $\boldsymbol{\varphi}(\mathbf{c}) = (\varphi_1(\mathbf{c}), \varphi_2(\mathbf{c}), \ldots, \varphi_{N-1}(\mathbf{c})) = \mathbf{f}(\mathbf{c}) + \beta(\mathbf{c})\mathbf{1}$.

3.2. The N-component Cahn–Hilliard system — a nonlinear multigrid method

In this section, we develop a nonlinear Full Approximation Storage (FAS) multigrid method to solve the nonlinear discrete system at the implicit time level. The nonlinearity, $\boldsymbol{\varphi}(\mathbf{c})$, is treated using one step of Newton's iteration and a pointwise Gauss-Seidel relaxation scheme is used as the smoother in the multigrid method. See the reference text [30] for additional details. We use the same notations as this reference text.

Let us rewrite Eqs. (9) and (10) as follows.

$$N(\mathbf{c}^n, \mathbf{c}^{n+1}, \boldsymbol{\mu}^{n+\frac{1}{2}}) = (\boldsymbol{\phi}^n, \boldsymbol{\psi}^n),$$

where the nonlinear system operator (N) is defined as

$$N(\mathbf{c}^n, \mathbf{c}^{n+1}, \boldsymbol{\mu}^{n+\frac{1}{2}}) = \left(\frac{\mathbf{c}^{n+1}}{\Delta t} - \nabla_d \cdot (M^{n+\frac{1}{2}}\nabla_d\boldsymbol{\mu}^{n+\frac{1}{2}}),\ \boldsymbol{\mu}^{n+\frac{1}{2}} - \frac{1}{2}\boldsymbol{\varphi}(\mathbf{c}^{n+1}) + \frac{\epsilon^2}{2}\Delta_d\mathbf{c}^{n+1}\right)$$

and the source term is

$$(\boldsymbol{\phi}^n, \boldsymbol{\psi}^n) = \left(\frac{\mathbf{c}^n}{\Delta t}, \frac{1}{2}\boldsymbol{\varphi}(\mathbf{c}^n) - \frac{\epsilon^2}{2}\Delta_d\mathbf{c}^n\right).$$

In the following description of one *FAS* cycle, we assume a sequence of grids Ω_k (Ω_{k-1} is coarser than Ω_k by a factor of 2). Given the number ν of pre- and post- smoothing relaxation sweeps, an iteration step for the nonlinear multigrid method using the V-cycle is formally written as follows:

FAS multigrid cycle

$$\{\mathbf{c}_k^{m+1}, \boldsymbol{\mu}_k^{m+\frac{1}{2}}\} = FAScycle(k, \mathbf{c}_k^n, \mathbf{c}_k^m, \boldsymbol{\mu}_k^{m-\frac{1}{2}}, N_k, \boldsymbol{\phi}_k^n, \boldsymbol{\psi}_k^n, \nu) \quad \text{on } \Omega_k \text{ grid}.$$

That is, $\{\mathbf{c}_k^m, \boldsymbol{\mu}_k^{m-\frac{1}{2}}\}$ and $\{\mathbf{c}_k^{m+1}, \boldsymbol{\mu}_k^{m+\frac{1}{2}}\}$ are the approximations of $\{\mathbf{c}_k^{n+1}(x_i, y_j), \boldsymbol{\mu}_k^{n+\frac{1}{2}}(x_i, y_j)\}$ before and after an *FAScycle*. We set the initial guess, $\mathbf{c}_k^0 = \mathbf{c}_k^n$ and $\boldsymbol{\mu}_k^{-\frac{1}{2}} = \boldsymbol{\mu}_k^{n-\frac{1}{2}}$. Now, we define the *FAScycle*.

Step 1 — Presmoothing:

$$\{\bar{\mathbf{c}}_k^m,\ \bar{\boldsymbol{\mu}}_k^{m-\frac{1}{2}}\} = SMOOTH^{\nu}(\mathbf{c}_k^m, \boldsymbol{\mu}_k^{m-\frac{1}{2}}, N_k, \boldsymbol{\phi}_k^n, \boldsymbol{\psi}_k^n) \quad \text{on } \Omega_k \text{ grid}.$$

This means performing ν smoothing steps with initial approximations $\mathbf{c}_k^m$ and $\boldsymbol{\mu}_k^{m-\frac{1}{2}}$ to get the approximation $\{\bar{\mathbf{c}}_k^m, \bar{\boldsymbol{\mu}}_k^{m-\frac{1}{2}}\}$. First, let us discretize Eq. (9) as a Gauss-Seidel type.

$$\frac{\bar{\mathbf{c}}_{ij}^m}{\Delta t} + \frac{M_{i+\frac{1}{2},j} + M_{i-\frac{1}{2},j} + M_{i,j+\frac{1}{2}} + M_{i,j-\frac{1}{2}}}{h^2}\bar{\boldsymbol{\mu}}_{ij}^{m-\frac{1}{2}} = \boldsymbol{\phi}_{ij}^n + \frac{M_{i+\frac{1}{2},j}\boldsymbol{\mu}_{i+1,j}^{m-\frac{1}{2}} + M_{i-\frac{1}{2},j}\bar{\boldsymbol{\mu}}_{i-1,j}^{m-\frac{1}{2}} + M_{i,j+\frac{1}{2}}\boldsymbol{\mu}_{i,j+1}^{m-\frac{1}{2}} + M_{i,j-\frac{1}{2}}\bar{\boldsymbol{\mu}}_{i,j-1}^{m-\frac{1}{2}}}{h^2}, \tag{11}$$

where $M_{i+\frac{1}{2},j} = M((\mathbf{c}_{ij}^m + \mathbf{c}_{i+1,j}^m + \mathbf{c}_{ij}^n + \mathbf{c}_{i+1,j}^n)/4)$ and the other terms are similarly defined. Next, let us discretize Eq. (10). Since $\boldsymbol{\varphi}(\mathbf{c}_{ij}^{n+1})$ is nonlinear with respect to $\mathbf{c}_{ij}^{n+1}$, we linearize $\boldsymbol{\varphi}(\mathbf{c}_{ij}^{n+1})$ at $\mathbf{c}_{ij}^m$, i.e.,

$$\boldsymbol{\varphi}(\mathbf{c}_{ij}^{n+1}) \approx \boldsymbol{\varphi}(\mathbf{c}_{ij}^m) + (\bar{\mathbf{c}}_{ij}^m - \mathbf{c}_{ij}^m)\frac{\partial \boldsymbol{\varphi}(\mathbf{c}_{ij}^m)}{\partial \mathbf{c}}, \tag{12}$$

where

$$\frac{\partial \boldsymbol{\varphi}(\mathbf{c}_{ij}^m)}{\partial \mathbf{c}} = \begin{pmatrix} \frac{\partial \varphi_1}{\partial c_1}(\mathbf{c}_{ij}^m) & \frac{\partial \varphi_2}{\partial c_1}(\mathbf{c}_{ij}^m) & \cdots & \frac{\partial \varphi_{N-1}}{\partial c_1}(\mathbf{c}_{ij}^m) \\ \frac{\partial \varphi_1}{\partial c_2}(\mathbf{c}_{ij}^m) & \frac{\partial \varphi_2}{\partial c_2}(\mathbf{c}_{ij}^m) & \cdots & \frac{\partial \varphi_{N-1}}{\partial c_2}(\mathbf{c}_{ij}^m) \\ \vdots & \vdots & \ddots & \vdots \\ \frac{\partial \varphi_1}{\partial c_{N-1}}(\mathbf{c}_{ij}^m) & \frac{\partial \varphi_2}{\partial c_{N-1}}(\mathbf{c}_{ij}^m) & \cdots & \frac{\partial \varphi_{N-1}}{\partial c_{N-1}}(\mathbf{c}_{ij}^m) \end{pmatrix}.$$

Then, putting Eq. (12) in Eq. (10) results in

$$-\bar{\mathbf{c}}_{ij}^m\left(\frac{\partial \boldsymbol{\varphi}(\mathbf{c}_{ij}^m)}{2\partial \mathbf{c}} + \frac{2\epsilon^2}{h^2}\right) + \bar{\boldsymbol{\mu}}_{ij}^{m-\frac{1}{2}} = \boldsymbol{\psi}_{ij}^n + \frac{1}{2}\boldsymbol{\varphi}(\mathbf{c}_{ij}^m) - \mathbf{c}_{ij}^m\frac{\partial \boldsymbol{\varphi}(\mathbf{c}_{ij}^m)}{2\partial \mathbf{c}} - \frac{\epsilon^2}{2h^2}(\mathbf{c}_{i+1,j}^m + \bar{\mathbf{c}}_{i-1,j}^m + \mathbf{c}_{i,j+1}^m + \bar{\mathbf{c}}_{i,j-1}^m). \tag{13}$$

One *SMOOTH* relaxation operator step consists of solving the system (11) and (13) by a $2(N-1) \times 2(N-1)$ matrix inversion for each ij. For example, as in our numerical tests in Section 4, for $N = 4$ case, we can rewrite Eqs. (11) and (13) as a matrix form:

$$\begin{pmatrix} a_{11} & 0 & 0 & a_{14} & 0 & 0 \\ 0 & a_{22} & 0 & 0 & a_{25} & 0 \\ 0 & 0 & a_{33} & 0 & 0 & a_{36} \\ a_{41} & a_{42} & a_{43} & a_{44} & 0 & 0 \\ a_{51} & a_{52} & a_{53} & 0 & a_{55} & 0 \\ a_{61} & a_{62} & a_{63} & 0 & 0 & a_{66} \end{pmatrix}\begin{pmatrix} \bar{c_1}_{ij}^m \\ \bar{c_2}_{ij}^m \\ \bar{c_3}_{ij}^m \\ \bar{\mu_1}_{ij}^{m-\frac{1}{2}} \\ \bar{\mu_2}_{ij}^{m-\frac{1}{2}} \\ \bar{\mu_3}_{ij}^{m-\frac{1}{2}} \end{pmatrix} = \begin{pmatrix} \bar{\phi_1}_{ij}^n \\ \bar{\phi_2}_{ij}^n \\ \bar{\phi_3}_{ij}^n \\ \bar{\psi_1}_{ij}^n \\ \bar{\psi_2}_{ij}^n \\ \bar{\psi_3}_{ij}^n \end{pmatrix}, \tag{14}$$

where

$$\begin{aligned} a_{11} &= 1/\Delta t, \\ a_{14} &= (M_{i+\frac{1}{2},j} + M_{i-\frac{1}{2},j} + M_{i,j+\frac{1}{2}} + M_{i,j-\frac{1}{2}})/h^2, \\ a_{41} &= -0.5\partial\boldsymbol{\varphi}(\mathbf{c}_{ij}^m)/\partial c_1 - 2\epsilon^2/h^2, \\ a_{42} &= -0.5\partial\boldsymbol{\varphi}(\mathbf{c}_{ij}^m)/\partial c_2, \\ a_{43} &= -0.5\partial\boldsymbol{\varphi}(\mathbf{c}_{ij}^m)/\partial c_3, \\ a_{44} &= 1, \end{aligned}$$

and the other terms are similarly defined. Also, the right hand side of Eq. (14) is the right hand side terms in Eqs. (11) and (13). Next, we will show that Eq. (14) is always invertible. An $n \times n$ matrix A is strictly diagonally dominant when

$$|a_{ii}| > \sum_{\substack{j=1, \\ j\neq i}}^{n} |a_{ij}| \tag{15}$$

holds for each $i = 1, 2, \ldots, n$. And a strictly diagonally dominant matrix A is nonsingular [5]. By using the method of Lagrange multipliers, we can easily find the maximum value of $M(\mathbf{c}) = \sum_{i<j}^4 c_i c_j$ subject to the constraint, $\sum_{i=1}^4 c_i = 1$. That is, when $c_1 = c_2 = c_3 = c_4 = 1/4$, the maximum value of $M(\mathbf{c})$ is 3/8. Therefore, $|a_{11}| > |0| + |0| + |a_{14}| + |0| + |0|$ for $\Delta t < 2h^2/3$. The maximum values of $|0.5\partial\boldsymbol{\varphi}(\mathbf{c}_{ij}^m)/\partial c_1|$, $|0.5\partial\boldsymbol{\varphi}(\mathbf{c}_{ij}^m)/\partial c_2|$, and $|0.5\partial\boldsymbol{\varphi}(\mathbf{c}_{ij}^m)/\partial c_3|$ are 1/4, 3/32, and 3/32, respectively. An equilibrium solution [23] of Eq. (6) in the infinite domain is

$$c_{1eq}(x) = \frac{1}{2}\left(1 + \tanh\left(\frac{x}{2\sqrt{2}\epsilon}\right)\right).$$

We define the interface thickness to be the distance from $c_{1eq} = 0.05$ to $c_{1eq} = 0.95$ so that the equilibrium interface thickness is $4\sqrt{2}\epsilon \tanh^{-1}(0.9)$. Numerically, we want to have four or five grid points across the interface transition. Let $4\sqrt{2}\epsilon \tanh^{-1}(0.9) \approx 4h$, then $\epsilon \approx h/(\sqrt{2}\tanh^{-1}(0.9)) \approx h/2.08203$. Therefore, the maximum value of $|2\epsilon^2/h^2|$ is less than $1/2$ for $\epsilon \leq h/2$. Therefore, $|a_{44}| = 1 > 15/16 \geq |a_{41}| + |a_{42}| + |a_{43}| + |0| + |0|$. In the same way, the inequality Eq. (15) is satisfied for $i = 2, 3, 5,$ and 6. Therefore, the matrix (14) is strictly diagonally dominant, i.e., nonsingular.

Step 2 — *Compute the defect:* $(\overline{\mathbf{def}}^m_{1\,k}, \overline{\mathbf{def}}^m_{2\,k}) = (\boldsymbol{\phi}^n_k, \boldsymbol{\psi}^n_k) - N_k(\mathbf{c}^n_k, \bar{\mathbf{c}}^m_k, \bar{\boldsymbol{\mu}}_k^{m-\frac{1}{2}})$.

Step 3 — *Restrict the defect and* $\{\bar{\mathbf{c}}^m_k, \bar{\boldsymbol{\mu}}_k^{m-\frac{1}{2}}\}$:

$$(\overline{\mathbf{def}}^m_{1\,k-1}, \overline{\mathbf{def}}^m_{2\,k-1}, \bar{\mathbf{c}}^m_{k-1}, \bar{\boldsymbol{\mu}}_{k-1}^{m-\frac{1}{2}}) = I_k^{k-1}(\overline{\mathbf{def}}^m_{1\,k}, \overline{\mathbf{def}}^m_{2\,k}, \bar{\mathbf{c}}^m_k, \bar{\boldsymbol{\mu}}_k^{m-\frac{1}{2}}).$$

The restriction operator I_k^{k-1} maps k-level functions to $(k-1)$-level functions. That is, coarse grid values are obtained by averaging the four nearby fine grid values.

Step 4 — *Compute the right-hand side:*

$$(\boldsymbol{\phi}^n_{k-1}, \boldsymbol{\psi}^n_{k-1}) = (\overline{\mathbf{def}}^m_{1\,k-1}, \overline{\mathbf{def}}^m_{2\,k-1}) + N_{k-1}(\mathbf{c}^n_{k-1}, \bar{\mathbf{c}}^m_{k-1}, \bar{\boldsymbol{\mu}}_{k-1}^{m-\frac{1}{2}}).$$

Step 5 — *Compute an approximate solution* $\{\hat{\mathbf{c}}^m_{k-1}, \hat{\boldsymbol{\mu}}_{k-1}^{m-\frac{1}{2}}\}$ *of the coarse grid equation on* Ω_{k-1}:

$$N_{k-1}(\mathbf{c}^n_{k-1}, \mathbf{c}^m_{k-1}, \boldsymbol{\mu}_{k-1}^{m-\frac{1}{2}}) = (\boldsymbol{\phi}^n_{k-1}, \boldsymbol{\psi}^n_{k-1}). \tag{16}$$

If $k = 1$, we apply the smoothing procedure in *Step* 1 to obtain the approximate solution. If $k > 1$, we solve (16) by performing a *FASk*-grid cycle using $\{\bar{\mathbf{c}}^m_{k-1}, \bar{\boldsymbol{\mu}}_{k-1}^{m-\frac{1}{2}}\}$ as an initial approximation:

$$\{\hat{\mathbf{c}}^m_{k-1}, \hat{\boldsymbol{\mu}}_{k-1}^{m-\frac{1}{2}}\} = FAScycle(k-1, \mathbf{c}^n_{k-1}, \bar{\mathbf{c}}^m_{k-1}, \bar{\boldsymbol{\mu}}_{k-1}^{m-\frac{1}{2}}, N_{k-1}, \boldsymbol{\phi}^n_{k-1}, \boldsymbol{\psi}^n_{k-1}, \nu).$$

Step 6 — *Compute the coarse grid correction (CGC):*

$$\hat{\mathbf{v}}^m_{k-1} = \hat{\mathbf{c}}^m_{k-1} - \bar{\mathbf{c}}^m_{k-1}, \quad \hat{\mathbf{w}}^{m-\frac{1}{2}}_{k-1} = \hat{\boldsymbol{\mu}}_{k-1}^{m-\frac{1}{2}} - \bar{\boldsymbol{\mu}}_{k-1}^{m-\frac{1}{2}}.$$

Step 7 — *Interpolate the correction:* $(\hat{\mathbf{v}}^m_k, \hat{\mathbf{w}}_k^{m-\frac{1}{2}}) = I^k_{k-1}(\hat{\mathbf{v}}^m_{k-1}, \hat{\mathbf{w}}_{k-1}^{m-\frac{1}{2}})$.

The interpolation operator I^k_{k-1} maps $(k-1)$-level functions to k-level functions. Here, the coarse values are simply transferred to the four nearby fine grid points.

Step 8 — *Compute the corrected approximation on* Ω_k:

$$\mathbf{c}_k^{m,\,\text{after CGC}} = \bar{\mathbf{c}}^m_k + \hat{\mathbf{v}}^m_k, \quad \boldsymbol{\mu}_k^{m-\frac{1}{2},\,\text{after CGC}} = \bar{\boldsymbol{\mu}}_k^{m-\frac{1}{2}} + \hat{\mathbf{w}}_k^{m-\frac{1}{2}}.$$

Step 9 — *Postsmoothing:*

$$\{\mathbf{c}^{m+1}_k, \boldsymbol{\mu}_k^{m+\frac{1}{2}}\} = SMOOTH^{\nu}(\mathbf{c}^n_k, \mathbf{c}_k^{m,\,\text{after CGC}}, \boldsymbol{\mu}_k^{m-\frac{1}{2},\,\text{after CGC}}, N_k, \boldsymbol{\phi}^n_k, \boldsymbol{\psi}^n_k) \text{ on } \Omega_k \text{ grid}.$$

This completes the description of a nonlinear *FAScycle*.

4. Numerical experiments — the quaternary Cahn–Hilliard system

In this section, we perform numerical experiments such as a convergence test, a linear stability analysis, the evolution of triple junctions, and phase separation in a four component mixture. The extensions to higher systems than a quaternary system are algebraically complex but conceptually straightforward.

The composition of a quaternary mixture (A, B, C, and D) can be mapped onto an equilateral tetrahedron whose corners represent a 100% concentration of A, B, C or D as shown in Fig. 1(a). Mixtures with components lying on planes parallel to the triangle, ΔBCD contain the same percentage of A: those with planes parallel to the triangle, ΔCDA have the same percentage of B concentration: and analogously for the C and the D concentrations. In Fig. 1(a) and (b), the mixture at the position marked '○' contains 20% A, $0.8 \times 30\%$ B, $0.8 \times 60\%$ C, and $0.8 \times 10\%$ D.

4.1. Convergence test

To obtain an estimate of the convergence rate, we perform a number of simulations for a sample initial problem on a set of increasingly finer grids. The initial conditions are

$$c_1(x, 0) = 0.25 + 0.01\cos(3\pi x) + 0.04\cos(5\pi x),$$
$$c_2(x, 0) = 0.25 - 0.02\cos(2\pi x) + 0.01\cos(4\pi x),$$
$$c_3(x, 0) = 0.25 + 0.03\cos(5\pi x) + 0.015\cos(3\pi x)$$

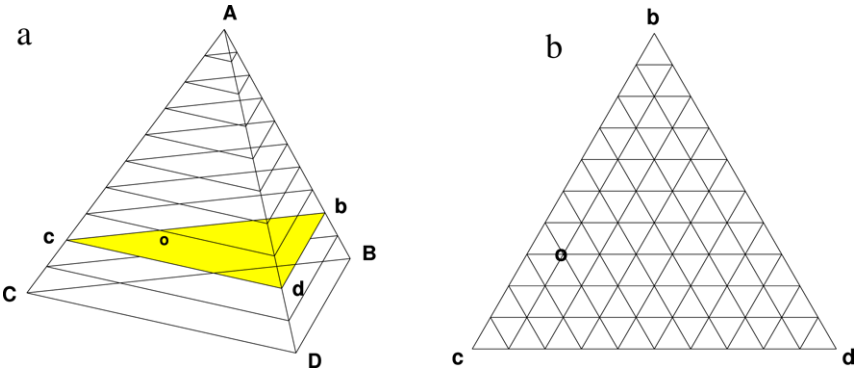

Fig. 1. Gibbs tetrahedron.

Table 1
l_2 convergence result

32–64	Rate	64–128	Rate	128–256	Rate	256–512
2.7910e−2	2.1412	6.3270e−3	2.0393	1.5393e−3	2.0103	3.8206e−4

on a domain, $\Omega = [0, 1]$. The numerical solutions are computed on the uniform grids, $h = 1/2^n$, and with corresponding time steps, $\Delta t = 0.1$ h for $n = 5, 6, 7, 8$, and 9. The calculations are run up to time $T = 0.1$ and $\epsilon = 0.005$ is used.

We define the error to be the discrete l_2-norm of the difference between that grid and the average of the next finer grid cells covering it: $\mathbf{e}_{h/\frac{h}{2}\,i} := \mathbf{c}_{hi} - (\mathbf{c}_{\frac{h}{2}\,2i} + \mathbf{c}_{\frac{h}{2}\,2i-1})/2$. The rate of convergence is defined as: $\log_2(\|\mathbf{e}_{h/\frac{h}{2}}\|/\|\mathbf{e}_{\frac{h}{2}/\frac{h}{4}}\|)$.

The errors and rates of convergence are given in Table 1. The results suggest that the scheme is indeed second order accurate.

4.2. Linear stability analysis

In this section, we study the short-time behavior of a quaternary mixture. The partial differential Eqs. (5) and (6) we wish to solve may be written as

$$\frac{\partial \mathbf{c}(x,t)}{\partial t} = \Delta\left(\boldsymbol{\varphi}(\mathbf{c}) - \epsilon^2 \Delta \mathbf{c}\right), \quad \text{where } (x,t) \in \Omega \times (0,T]. \tag{17}$$

Let the mean concentration take the form $\mathbf{m} = (m_1, m_2, m_3)$. We seek a solution of the form

$$\mathbf{c}(x,t) = \mathbf{m} + \sum_{k=1}^{\infty} \cos(k\pi x)(\alpha_k(t), \beta_k(t), \gamma_k(t)), \tag{18}$$

where $|\alpha_k(t)|$, $|\beta_k(t)|$, and $|\gamma_k(t)| \ll 1$. After linearizing $\boldsymbol{\varphi}(\mathbf{c})$ about $\mathbf{m}$, we have

$$\boldsymbol{\varphi}(\mathbf{c}) \approx \boldsymbol{\varphi}(\mathbf{m}) + (\mathbf{c} - \mathbf{m}) \begin{pmatrix} \partial_{c_1}\varphi_1(\mathbf{m}) & \partial_{c_1}\varphi_2(\mathbf{m}) & \partial_{c_1}\varphi_3(\mathbf{m}) \\ \partial_{c_2}\varphi_1(\mathbf{m}) & \partial_{c_2}\varphi_2(\mathbf{m}) & \partial_{c_2}\varphi_3(\mathbf{m}) \\ \partial_{c_3}\varphi_1(\mathbf{m}) & \partial_{c_3}\varphi_2(\mathbf{m}) & \partial_{c_3}\varphi_3(\mathbf{m}) \end{pmatrix}. \tag{19}$$

Substituting (19) into (17) and letting $m_1 = m_2 = m_3 = m$ for simplicity, then, up to first order, we have

$$\frac{\partial \mathbf{c}}{\partial t} = \Delta \mathbf{c} \begin{pmatrix} \frac{18m^2 - 9m + 1}{2} & \frac{3m(4m-1)}{2} & \frac{3m(4m-1)}{2} \\ \frac{3m(4m-1)}{2} & \frac{18m^2 - 9m + 1}{2} & \frac{3m(4m-1)}{2} \\ \frac{3m(4m-1)}{2} & \frac{3m(4m-1)}{2} & \frac{18m^2 - 9m + 1}{2} \end{pmatrix} - \epsilon^2 \Delta^2 \mathbf{c}. \tag{20}$$

After substituting $\mathbf{c}(x,t)$ from Eq. (18) into (20), we get

$$\begin{pmatrix} \alpha_k(t) \\ \beta_k(t) \\ \gamma_k(t) \end{pmatrix}' = \mathbf{A} \begin{pmatrix} \alpha_k(t) \\ \beta_k(t) \\ \gamma_k(t) \end{pmatrix}, \qquad \mathbf{A} = \begin{pmatrix} a & b & b \\ b & a & b \\ b & b & a \end{pmatrix}, \tag{21}$$

where $'$ indicates the time derivative and

$$a = \frac{-k^2\pi^2}{2}(18m^2 - 9m + 1) - \epsilon^2 k^4 \pi^4, \qquad b = \frac{-3k^2\pi^2 m(4m-1)}{2}.$$

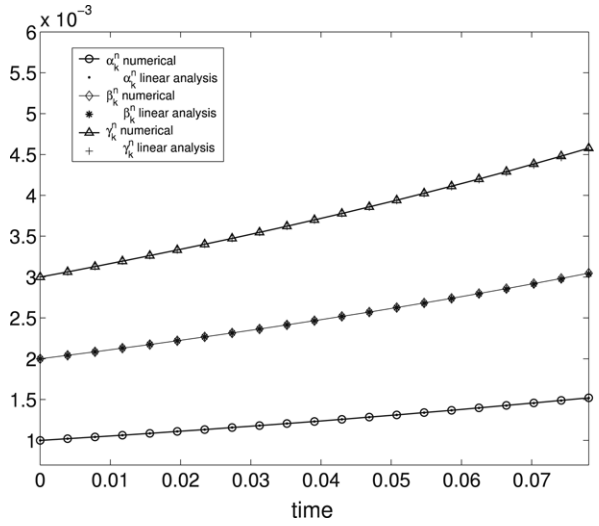

Fig. 2. The symbols '-o-', '-◇-', and '-△-' are numerical results that we are compared with the theoretical values $\alpha_k(t)$ (point), $\beta_k(t)$ (star), and $\gamma_k(t)$ (plus), respectively, with the initial conditions of Eqs. (22)–(24).

The eigenvalues of **A** are

$$\lambda_1 = -\frac{k^2\pi^2}{2}(42m^2 - 15m + 1 + 2\epsilon^2 k^2\pi^2),$$
$$\lambda_2 = \lambda_3 = -\frac{k^2\pi^2}{2}(6m^2 - 6m + 1 + 2\epsilon^2 k^2\pi^2).$$

The solution to the system of *ODEs* (21) is given by

$$\begin{pmatrix}\alpha_k(t)\\ \beta_k(t)\\ \gamma_k(t)\end{pmatrix} = \frac{\alpha_k(0)+\beta_k(0)+\gamma_k(0)}{3}\begin{pmatrix}1\\1\\1\end{pmatrix}e^{\lambda_1 t} + \frac{-\alpha_k(0)-\beta_k(0)+2\gamma_k(0)}{3}\begin{pmatrix}-1\\0\\1\end{pmatrix}e^{\lambda_2 t}$$
$$+\frac{-\alpha_k(0)+2\beta_k(0)-\gamma_k(0)}{3}\begin{pmatrix}-1\\1\\0\end{pmatrix}e^{\lambda_2 t}.$$

In Fig. 2, we plot the evolution of the amplitudes as a function of time. The symbols '-o-', '-◇-', and '-△-' are numerical results that we are compared with the theoretical values $\alpha_k(t)$ (point), $\beta_k(t)$ (star), and $\gamma_k(t)$ (plus), respectively, with the initial conditions:

$$c_1(x,0) = 0.25 + 0.001\cos(3\pi x), \tag{22}$$
$$c_2(x,0) = 0.25 + 0.002\cos(3\pi x), \tag{23}$$
$$c_3(x,0) = 0.25 + 0.003\cos(3\pi x). \tag{24}$$

Here, we used $k = 3$, $m = 0.25$, $\epsilon = 0.005$, $h = 1/256$, $\Delta t = 0.1$ h, and $T = 200\Delta t$. The numerical amplitudes are defined by

$$\alpha_k^n = \left(\max_{1\le i\le N_x} c_1^n(x_i) - \min_{1\le i\le N_x} c_1^n(x_i)\right)\Big/2,$$
$$\beta_k^n = \left(\max_{1\le i\le N_x} c_2^n(x_i) - \min_{1\le i\le N_x} c_2^n(x_i)\right)\Big/2,$$
$$\gamma_k^n = \left(\max_{1\le i\le N_x} c_3^n(x_i) - \min_{1\le i\le N_x} c_3^n(x_i)\right)\Big/2.$$

The results in Fig. 2 show that the linear stability analysis and numerical solutions are in good agreement in a linear regime.

4.3. Triple junctions in a quaternary system

For a quaternary system, we calculate the evolution of triple junctions. In the first experiment for triple junctions, see Fig. 3(a), we simulate how two T-shaped triple junctions approach a local equilibrium state. The initial angles at the triple

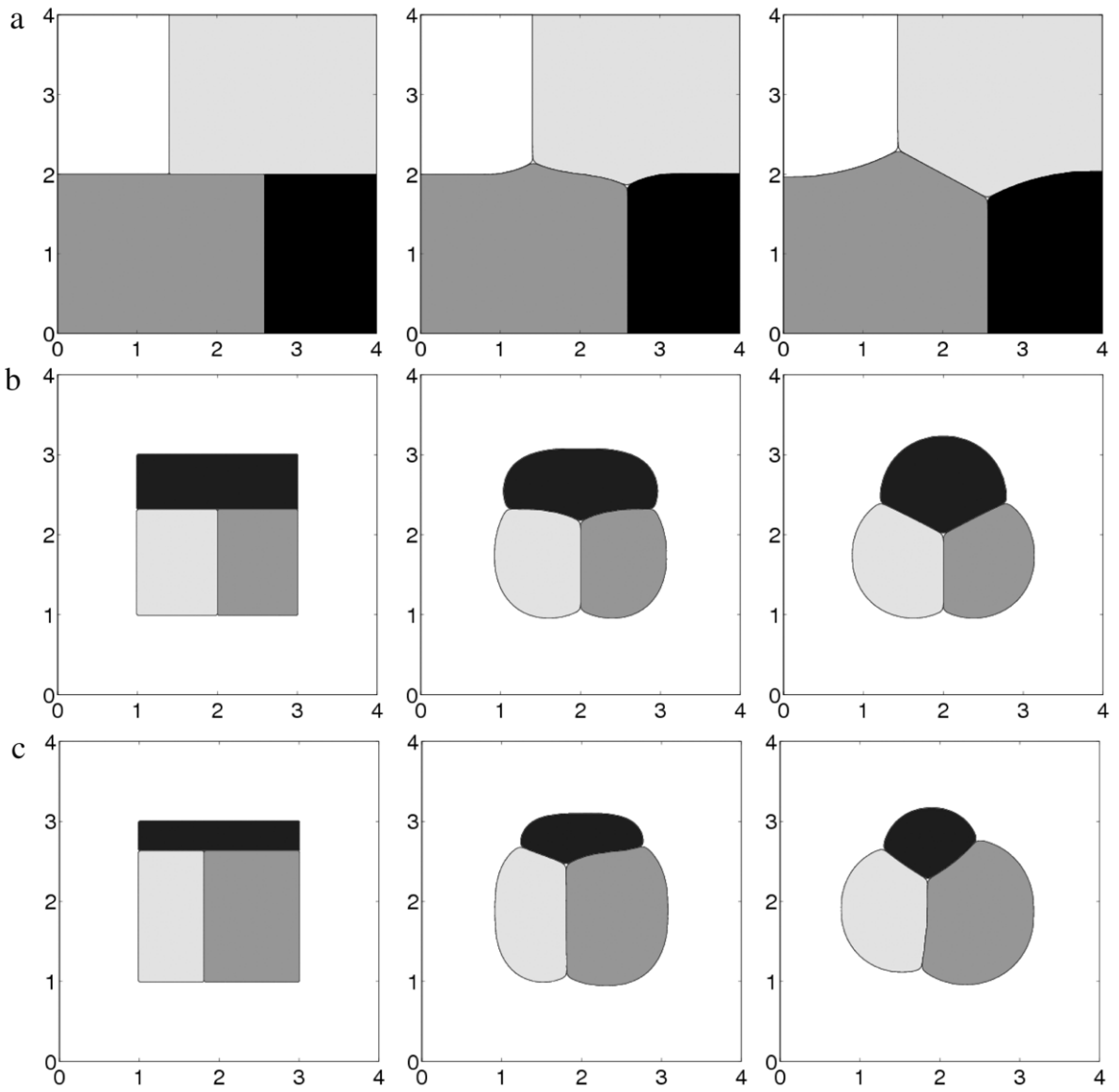

Fig. 3. Temporal evolution of triple junctions. The times are $t = 0$, 15.63, and 390.63 (from left to right). Phase A is represented by the white region, phase B by the gray region, phase C by the dark gray region, and phase D by the black region.

points are 90° and 180°. A 128 × 128 grid is used on the interval $\Omega = [0, 4] \times [0, 4]$. We choose $h = 4/128$, $\Delta t = 0.4$ h, and $\epsilon = 0.01$. We compute until the solution becomes numerically stationary. In Fig. 3 we display the evolution of the interface at different times. The times are $t = 0$, 15.63, and 390.63 (from left to right). Phase A is represented by the white region, phase B by the gray region, phase C by the dark gray region, and phase D by the black region. The second experiment starts with three equal rectangular areas (Fig. 3(b)). In the third experiment, we simulate a non equal area case (Fig. 3(c)).

We note that for the three cases' experiments, we observe that the triple junction angles approach the true value 120° as they approach local equilibrium states. This is due to the fact that in the total energy functional equation (2), $\mathcal{F}(\mathbf{c}(\mathbf{x}, t))$ is symmetric and the interaction parameter ϵ is constant.

4.4. One dimensional spinodal decomposition — the phase separation of a four-component mixture

We perform a spinodal decomposition with the initial conditions:

$$c_1(x, 0) = m_1 + 0.01\text{rand}(x),$$
$$c_2(x, 0) = m_2 + 0.01\text{rand}(x),$$
$$c_3(x, 0) = m_3 + 0.01\text{rand}(x),$$

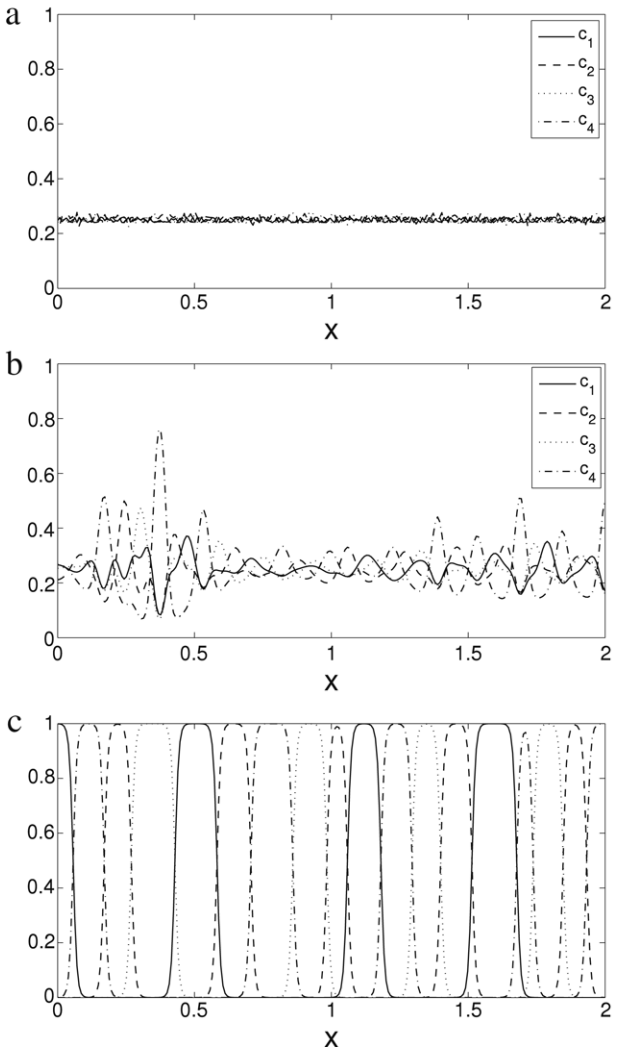

Fig. 4. Time evolution of a quaternary system with average concentrations $\mathbf{m} = (m_1, m_2, m_3) = (\frac{1}{4}, \frac{1}{4}, \frac{1}{4})$ at time $t = 0.0, 0.08,$ and 39.06 (from top to bottom). The solid, dashed, dotted, and dash-dot lines are c_1, c_2, c_3, and $c_4 = 1 - c_1 - c_2 - c_3$, respectively.

where the mean concentration, $\mathbf{m} = (m_1, m_2, m_3) = (1/4, 1/4, 1/4)$. The random number rand$(x)$ is in $[-1, 1]$ and has zero mean. Some disturbance to the initially uniform concentrations is needed since $\mathbf{c} = \mathbf{m}$ satisfies a local equilibrium solution to Eqs. (9) and (10). The random disturbance is believed to be a physically reasonable approximation to thermal noise. A 256 grid is used on the interval $\Omega = [0, 2]$. We choose $h = 2/256$, $\Delta t = 0.1$ h, and $\epsilon = 0.005$. We arranged the pictures in Fig. 4 with time increasing from the top to the bottom ($t = 0.0$, 0.08, and 39.06). The solid, dashed, dotted, and dash-dot lines are c_1, c_2, c_3, and $c_4 = 1 - c_1 - c_2 - c_3$, respectively. The variable Lagrange multiplier $\beta(\mathbf{c})$, Eq. (4), ensures that there is no presence of the third phase at a two phase boundary when the mixture is close to an equilibrium state (Fig. 4(c)).

4.5. Two dimensional spinodal decomposition — the phase separation of a four-component mixture

Next, we study a phase separation via a spinodal decomposition of a quaternary mixture. In the simulations, the initial conditions were random perturbations of maximum amplitude 0.05 of the uniform state $\mathbf{c} = \mathbf{m}$. The average compositions of the first three phases were equal and the average composition of the fourth phase was varied. A 128×128 mesh was used on the square domain $\Omega = [0, 4] \times [0, 4]$ for the spatial discretization and a time step, $\Delta t = 1/128$ was employed for the time integration. We took $\epsilon = 0.015$.

In the first experiment, the initial conditions were random perturbations of the uniform state $\mathbf{m} = (1/4, 1/4, 1/4)$. The results are presented in Fig. 5(a). The area shown in white indicates the A phase region, while the gray, dark gray, and black color regions stand for the B-rich, C-rich and D-rich domains, respectively. Since the composition is completely symmetric with respect to the four components, all four phases have similar morphologies and evolution dynamics [8].

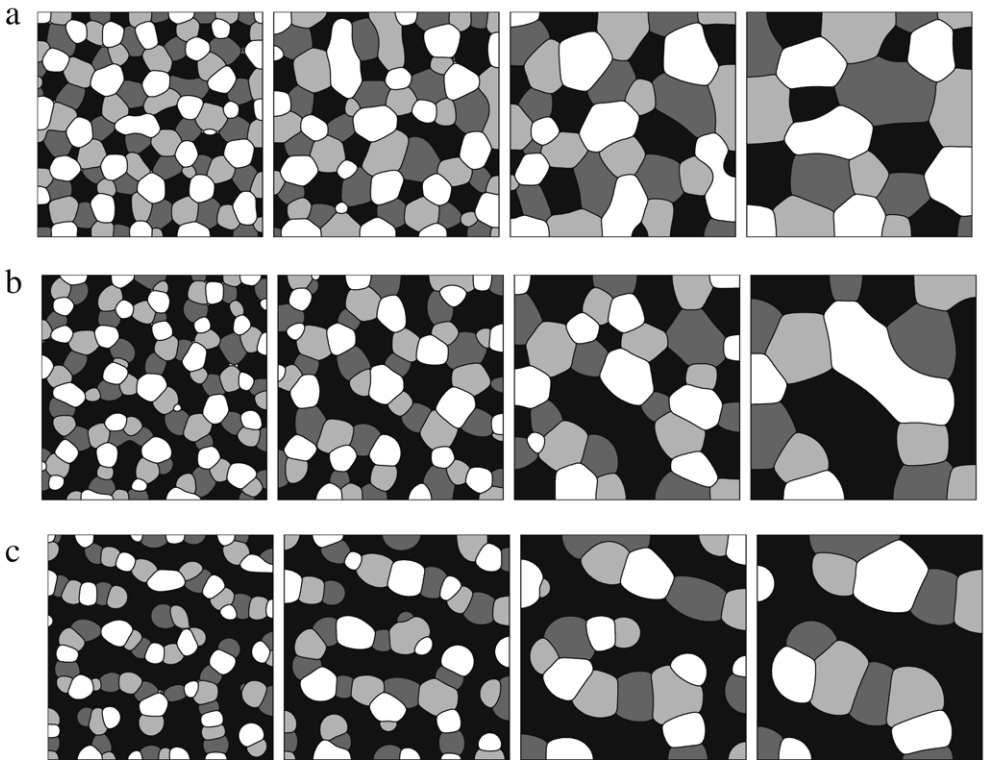

Fig. 5. The temporal evolution of morphologies during a spinodal phase separation of a quaternary system with average composition (a) $\mathbf{m} = (1/4, 1/4, 1/4)$, (b) $\mathbf{m} = (1/5, 1/5, 1/5)$, and (c) $\mathbf{m} = (1/6, 1/6, 1/6)$, respectively. Times are $t = 4.69$, 11.72, 39.84, and 117.19 (from left to right). Phase A is represented by the white region, phase B by the gray region, phase C by the dark gray region, and phase D by the black region.

In the second experiment with $\mathbf{m} = (1/5, 1/5, 1/5)$, Fig. 5(b) shows the time evolution of the quaternary system. We observe four phases in the early stages of spinodal decomposition. As shown for time $t = 4.69$, the $c_1 + c_2 + c_3$ and c_4 phases appear as interconnected at the initial stages of decomposition, which is very similar to what is observed in binary systems.

In the third experiment with $\mathbf{m} = (1/6, 1/6, 1/6)$ (Fig. 5(c)), initially, we see four phases, one of them dominated by c_4. The evolution of the system is in the direction of $c_1 + c_2 + c_3$ and c_4.

4.6. Two dimensional spinodal decomposition — the phase separation of a four-component mixture with a variable mobility

The numerical test in this section highlights the effect of a concentration dependent mobility. To account for the different mobilities between different components, we consider a mobility $M(\mathbf{c})$ associated with all possible pairs of phases.

$$M(\mathbf{c}) = c_1c_2 + \frac{1}{3}c_1c_3 + \frac{1}{9}c_1c_4 + \frac{1}{27}c_2c_3 + \frac{1}{81}c_2c_4 + \frac{1}{243}c_3c_4. \tag{25}$$

A 256×256 mesh was used on the square domain $\Omega = [0, 8] \times [0, 8]$ for the spatial discretization and a time step, $\Delta t = 0.1/256$ was employed for the time integration. We took $\epsilon = 0.015$.

For the initial data, we used are shown in Fig. 6(a). Here, c_i and c_j mean that on that region, $c_i = 0.5 + 0.01\text{rand}(x, y)$ and $c_j = 1 - c_i$. In Fig. 6(b), the mobility $M(\mathbf{c})$, Eq. (25), is given at the initial time. Fig. 7 shows the temporal evolution of morphologies during a spinodal phase separation of a quaternary system with a concentration dependent mobility ((a) c_1, (b) c_2, (c) c_3, and (d) c_4). Rows 1 and 2 correspond to $t = 0.0977$ and 1.9531, respectively. As we expect from the form of the mobility $M(\mathbf{c})$, we find the morphology transitions in Fig. 7.

5. Conclusions

We considered a fully discrete semi-implicit finite difference scheme for the N-component CH system with a concentration dependent mobility and solved the resulting scheme by an efficient and accurate nonlinear multigrid method. We carried out numerical experiments such as a second-order convergence test, comparison with linear stability analysis, and evolution of triple junctions. We have also investigated phase separation via spinodal decomposition with a constant and degenerate concentration dependent mobilities in a quaternary system.

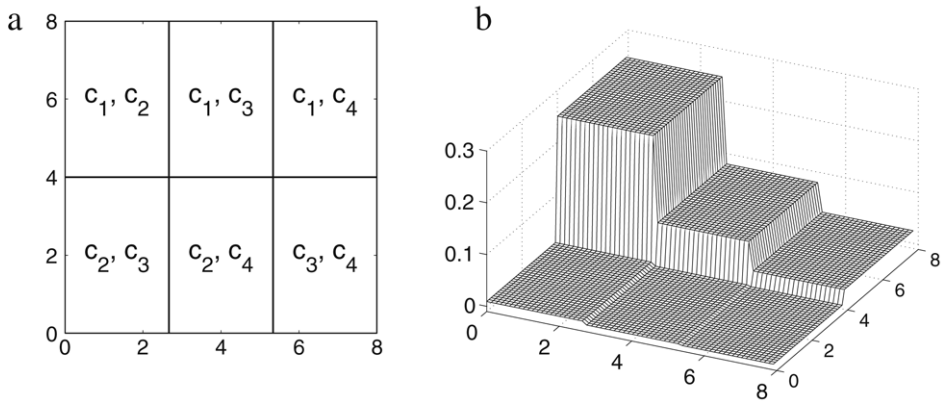

Fig. 6. (a) Initial configuration. (b) Mobility, $M(\mathbf{c})$ at time zero.

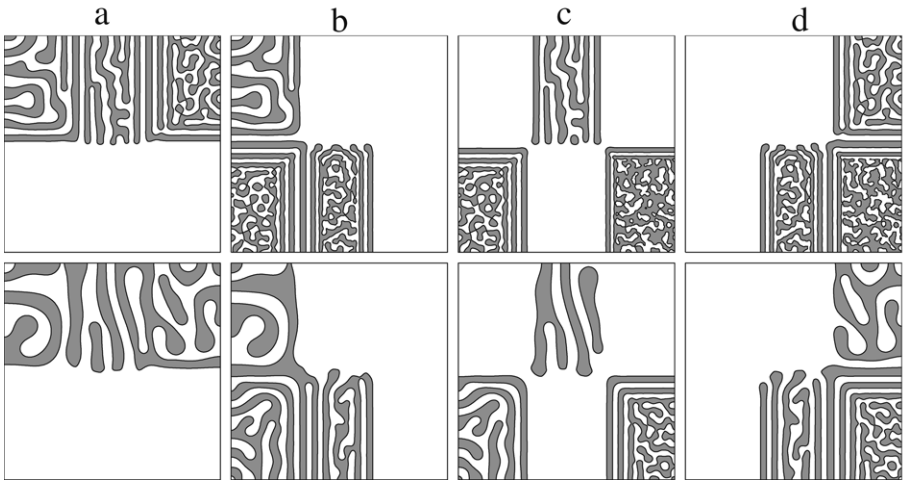

Fig. 7. The temporal evolution of morphologies during a spinodal phase separation of a quaternary system with a concentration dependent mobility ((a) c_1, (b) c_2, (c) c_3, and (d) c_4). Rows 1 and 2 correspond to $t = 0.0977$ and 1.9531, respectively.

Acknowledgments

This research was supported by the MKE (Ministry of Knowledge Economy), Korea, under the ITRC (Information Technology Research Center) support program supervised by the IITA (Institute for Information Technology Advancement) (IITA-2008- C1090-0801-0013). This work was also supported by the Korea Research Foundation Grant funded by the Korean Government (MOEHRD) (KRF-2006-C00225).

References

[1] S. Bhattacharyya, T.A. Abinandanan, Bull. Mater. Sci. 26 (2003) 193.
[2] J.W. Barrett, J.F. Blowey, Math. Comp. 68 (1999) 487.
[3] J.W. Barrett, J.F. Blowey, H. Garcke, M2AN Math. Model. Numer. Anal. 35 (2001) 713.
[4] J.F. Blowey, M.I.M. Copetti, C.M. Elliott, IMA J. Numer. Anal. 16 (1996) 111.
[5] Richard L. Burden, J. Douglas Faires, Numerical Analysis, Thomson Brooks/Cole, 2005.
[6] J.W. Cahn, Acta Metall. 9 (1961) 795.
[7] J.W. Cahn, J. Chem. Phys. 42 (1965) 93.
[8] L.Q. Chen, Scripta Metall. Mater. 29 (1993) 683.
[9] M.I.M. Copetti, Math. Comput. Simul. 52 (2000) 41.
[10] C.M. Elliott, in: J.F. Rodrigues (Ed.), Mathematical Models for Phase Change Problems, Birkhäuser Verlag, Basel, 1989.
[11] C.M. Elliott, D.A. French, SIAM J. Numer. Anal. 26 (1989) 884.
[12] C.M. Elliott, D.A. French, F. Milner, Numer. Math. 54 (1989) 575.
[13] C.M. Elliott, H. Garcke, Physica D 109 (1997) 242.
[14] C.M. Elliott, S. Larsson, Math. Comp. 58 (1992) 603.
[15] C.M. Elliott, S. Luckhaus, IMA, University of Minnesota, 1991, preprint 887.
[16] D.J. Eyre, SIAM J. Appl. Math. 53 (1993) 1686.
[17] D de Fontaine, A Computer Simulation of the Evolution of Coherent Composition Variations in Solid Solutions, Ph.D. Thesis, Northwestern University, 1967.

[18] D. Furihata, J. Comput. Phys. 156 (1999) 181.
[19] D. Furihata, Numer. Math. 87 (2001) 675.
[20] D.A. French, J.W. Schaeffer, Appl. Math. Comput. 39 (1990) 271.
[21] H. Garcke, B. Nestler, B. Stoth, Physica D 115 (1998) 87.
[22] J.E. Hilliard, Phase Transformations, American Society for Metals, Cleveland, 1970, p. 497.
[23] J.S. Kim, J. Comput. Phys. 204 (2005) 784.
[24] R. Kornhuber, R. Krause, Comput. Visual. Sci. 9 (2006) 103.
[25] J.S. Kim, K. Kang, J.S. Lowengrub, Comm. Math. Sci. 2 (2004) 53.
[26] J.E. Morral, J.W. Cahn, Acta Metall. 19 (1971) 1037.
[27] L. Mohamed, G.M. Ole, T. Søren, Phys. Rev. E 53 (1996) 3673.
[28] S. Maier-Paape, B. Stoth, T. Wanner, J. Statist. Phys. 98 (2000) 871.
[29] Z.Z. Sun, Math. Comp. 64 (1995) 1463.
[30] U. Trottenberg, C. Oosterlee, A. Schüller, MULTIGRID, Academic Press, 2001.
[31] J.D. van der Waals, J. Stat. Phys. 20 (1979) 197.